ROYAL SOCIETY OF CHEMISTRY

PAPER

Check for updates

3D-Printing of succulent plant-like scaffolds with beneficial cell microenvironments for bone regeneration†

Yufeng Wang,[ab] Zikang Wang,[b] Xiaopeng Yu,[b] Meng Zhang,[b] Xin Wang,[b] Yanling Zhou,[b] Qingqiang Yao*[a] and Chengtie Wu [ID] *[b]

Biomimetic materials with complicated structures inspired by natural plants play a critical role in tissue engineering. The succulent plants, with complicated morphologies, show tenacious vitality in extreme conditions due to the physiological functions endowed by their unique anatomical structures. Herein, inspired by the macroscopic structure of succulent plants, succulent plant-like bioceramic scaffolds were fabricated *via* digital laser processing 3D printing of $MgSiO_3$. Compared with conventional scaffolds with interlaced columns, the structures could prevent cells from leaking from the scaffolds and enhance cell adhesion. The scaffold morphology could be well regulated by changing leaf sizes, shapes, and interlacing methods. The succulent plant-like scaffolds show excellent properties for cell loading as well as cell distribution, promoting cellular interplay, and further enhancing the osteogenic differentiation of bone marrow stem cells. The *in vivo* study further illustrated that the succulent plant-like scaffolds could accelerate bone regeneration by inducing the formation of new bone tissues. The study suggests that the obtained succulent plant-like scaffold featuring the plant macroscopic structure is a promising biomaterial for regulating cell distribution, enhancing cellular interactions, and further improving bone regeneration.

10th Anniversary Statement

Supported by the Shanghai Institute of Ceramics, Chinese Academy of Sciences, our team has been committed to the research of inorganic non-metal biomaterials, focusing on the applications of various biomaterials such as 3D printed composite materials, multi-scale hierarchical materials, biomimetic materials, *etc.* Consistent with the scope of the honored *Journal of Materials Chemistry B* (JMCB), we have done series of research on material fabrication and applications in tissue regeneration, tumor treatment, drug delivery, *etc.* Over the past ten years, we have had close cooperation with JMCB and published over 10 papers, involving bioactive materials, biomimetic materials, regenerative medicine and 3D-printed scaffolds. Therefore, it is my great honor to win the Journal of Materials Chemistry Lectureship award in 2015, and outstanding reviewer for JMCB. We wish that the JMCB will continually enhance its global impact in the field of biomaterials. We will continue our efforts in the fabrication of advanced biomaterials and the research of biological properties to create more impressive scientific achievements together with this honored journal.

1 Introduction

Over millions of years, different plants have evolved sophisticated structures with corresponding functions for survival. Inspired by the sophisticated structures of different plants from the nanoscale to microscale, various biomimetic materials have been developed with hydrophilicity, high adhesion ability, or high compressive strength, which have been applied in many fields such as architecture, mechanics, and medicine. For example, the parallel channels of the lotus could accelerate air ventilation and nutrient exchange, which could be applied in bone tissue engineering scaffolds for cell delivery and osteogenesis.[1] The organized pericarp is composed of a multi-layered and multiscale structure, and the disordered mesocarp endows coconuts with crashworthiness, providing a plant-inspired template for the design of functionally graded composite materials.[2] The asymmetric wedge-shaped grooves of nepenthes could prevent fluid backflow to keep the moisture in the peristome organ, which could be applied in the drug delivery system.[3]

[a] *Department of Orthopaedic Surgery, Nanjing First Hospital, Nanjing Medical University, 210006, Nanjing, China. E-mail: yaoqingqiang@njmu.edu.cn*

[b] *State Key Laboratory of High Performance Ceramics and Superfine Microstructure, Shanghai Institute of Ceramics, Chinese Academy of Sciences, Shanghai, 200050, P. R. China. E-mail: chengtiewu@mail.sic.ac.cn*

† Electronic supplementary information (ESI) available. See DOI: **https://doi.org/10.1039/d2tb02056d**

This journal is © The Royal Society of Chemistry 2023

J. Mater. Chem. B, 2023, **11**, 5523–5536 | **5523**

Succulent plants are a type of terrestrial plant with various florae, which have unique anatomical structures and physiological functions for supporting life in extreme conditions. Succulent plants are classified into all-cell succulents and storage succulents. The former depicts the condition where the botanical cells could simultaneously store water and perform photosynthesis. While the latter represents the species that possess divided photosynthetic tissues and water storage tissues.[4,5] The all-cell succulents tend to have a large non-spheroid leaf to hold more water for photosynthesis and a low surface area-to-volume ratio (SA:V) to reduce transpiration.[4] In tissue engineering, an overall flat leaf structure with a large area could load more cells on scaffolds, and sustain more bioactive regulators produced *via* paracrine action, leading to more cellular interactions.[6] Moreover, a low SA:V could reduce the cell movement before cells adhere to the scaffolds, and thus reduce energy consumption.[7] In contrast, the storage succulents usually have a nearly spheroid leaf, which could avoid extra transpiration due to the small specific surface area of globular shapes.[4] This structure could be potentially applied in scaffold design to improve the spread of cells and stimulate the elongation of cells.

Diverse succulent plants differ in stem morphology, size, leaf shape, leaf size, and leaf thickness, leading to different capabilities of photosynthesis, water storage, and nutrient transportation. A large leaf could hold more water due to its high surface area. A thick leaf could maintain the temperature and reduce water evaporation under harsh environments. The unique stomatal and interlaced leaf structures also increase nutrition collection and storage. Moreover, interleaf distance also imposes a limitation on water transportation in different succulent plants.[8] Similarly, tissue engineering scaffolds require some favorable structural traits to support the regeneration process, such as enough mechanical strength, proper degradation profile, the release of bioactive components, and efficient nutrition transportation. The large leaf structure could provide enough space for cell adhesion and ECM deposition. The thick leaf structures could strengthen the mechanical properties. The interlaced structure could accelerate nutrition exchange and improve cellular interaction. As a result, suitable succulent plants have the ideal structure with high surface area, nutrition storage capacity, and an extended root system,[9] which could be potentially applied in bone tissue engineering for enhancing cell loading, cell adhesion, and intercellular crosstalk.

Previous studies have illustrated biomimetic structures inspired by the macroscopic structures of plants or animals in nature for biological application. For example, the structures of fish scales, lobster claws, antler bones, abalone nacre, and silica sponges are mimicked for enhancing the toughness of materials.[10,11] Bioinspired structures mimicking pine cones[12] and Bauhinia pods[13] have been constructed to imitate the shape-changing properties in nature. The macroscopic structure of the conch has been mimicked to fabricate scaffolds for guiding cell migration and bone growth.[14] Moreover, the structures of the human glomerulus, bone, and spinal cord have also inspired researchers to construct scaffolds with more functions.[15–17]

The implantation of bone tissue engineering scaffolds could enhance the repair of bone defects and it is an ingenious method for imitating the gross structure of succulent plants to fabricate a bone tissue engineering scaffold. Currently, the digital light processing (DLP) 3D printing technique, with the distinct advantages of high resolution, customization, easy modeling process, wide application, and acceptable cost, has been widely used to construct tissue engineering scaffolds with customized macroscopic structures.

In addition to the osteogenic effect of specialized structures, the material itself should possess the properties of good biocompatibility, osteoinduction, osteointegration, and osteogenesis. Magnesium silicate ($MgSiO_3$) bioceramics with the effects of enzymatic activation, immune modulation, enhancing cell proliferation, and improving osteogenesis,[18–21] could be applied as a bone substitute. Mg, as part of $Mg-ATP^{2-}$, is essential for sustaining protein synthesis, DNA duplication, and cytoskeleton rearrangement. Mg can also improve cell proliferation by accelerating mitotic spindle formation and cytokinesis.[22,23] In addition, Mg could regulate enzyme activity by modulating the core of metabolisms such as the Krebs cycle and the respiratory chain.[24] However, Mg deficiency may generate metabolic and energetic stress and lead to the accumulation of free radicals, which could upregulate stress proteins and the NF-κB pathway, thus activating inflammatory reactions.[25] Mg^{2+} ions could also improve osteogenesis by stimulating osteoblast differentiation and inhibiting osteoclast formation in a dose-dependent manner.[26,27] Silicon is an essential element for normal development and primarily exists in the bone-growing area, especially in osteoblasts. Silicate enhances bone growth by increasing bone water content with mineral deposition and improves cartilage formation by elevating the hexosamine and collagen content. Moreover, silicon and magnesium are contained in natural bone. Hence, $MgSiO_3$ is an appropriate material for the fabrication of bone scaffolds.[28]

In this study, inspired by the morphologies of succulent plants, succulent plant-like scaffolds with high-precision and sophisticated succulent plant-like structures were successfully fabricated with the DLP 3D printing technique. We systematically explored the effects of the overall shape, specific surface area, leaf shape, size, and interlacing method on bone regeneration. By regulating these parameters, the aim is to compare the capacity for cell recruitment, cell loading, cell proliferation, and osteogenic potentials of scaffolds with different structures. Notably, the obtained scaffolds could regulate cell distribution and cell density, and improve osteogenic effects compared with conventional layered 3D-printed scaffolds with vertical interlaced structures both *in vitro* and *in vivo*. Therefore, we provide the concept of a macro-appearance-imitating strategy and a feasible method for constructing biomimetic succulent plant-like scaffolds *via* DLP 3D printing for application in bone tissue engineering.

2 Experimental section

2.1 Design of the scaffolds

To design the scaffolds mimicking different succulent plants, 3ds Max (Autodesk) was applied to fabricate digital models and

5524 | *J. Mater. Chem. B*, 2023, **11**, 5523–5536

This journal is © The Royal Society of Chemistry 2023

then obtain the stereolithography (STL) files for the subsequent 3D printing. In detail, six types of succulent plants with different structures were chosen as the experimental groups, including Graptopetalum pachyphyllum, Maguey chato agave, Aeonium canariense, Astroloba, Sedum morganianum, and Echeveria jasiri by varying the size, shape, and interlacing method of leaves with stems. According to the six types of plants, the succulent plant-like scaffolds with spindle, pentagon, rose, triangle, ellipsoid, and sword leaf shapes were constructed.

The specific surface areas of all succulent plant-like models were obtained according to the automatically generated statistics by 3ds Max software. In addition, conventional scaffolds composed of vertical interlaced columns were chosen as the control group. The STL files of designed models were then imported into 10DIM (Beijing Ten Dimensions Technology Co. Ltd, China) software and then the TDP files were exported for the next DLP 3D printing process.

2.2 Fabrication of the scaffolds

The $MgSiO_3$ powders and bioactive glasses were provided by Kunshan Chinese Technology New Materials Co. Ltd (Kunshan, Jiangsu, China). Here, 57 g of $MgSiO_3$ powders and 3 g of 45S5 bioactive glass powders were mixed with 40 g of photosensitive resin (WANHAO Co. Ltd, Jinhua, Zhejiang, China) and ball milled (Nanjing NanDa Instrument Plant) to obtain the precursor slurry for the next DLP printing.

The succulent plant-like scaffolds were prepared by a DLP-based 3D printer (AUTOCERA-M, Beijing Ten Dimensions Technology Co. Ltd, China). In detail, 50 mL of the precursor slurry was added to the resin tank and then polymerized layer by layer. Afterwards, the samples were further cross-linked using 405 nm light. After finishing the printing process, the samples were washed in an ultrasonic washer with alcohol for 60 s to remove the residual resin. The scaffolds were dried overnight in a drying oven at 60 °C. The green body of the scaffold was then sintered at a set program to remove the solidified resin. The scaffolds were heated to 300 °C for 2 h at a heating rate of 2 °C min^{-1} and then heated to 650 °C for 2 h at a heating rate of 1 °C min^{-1}. Finally, the scaffolds were heated to 1360 °C for 4 h at a heating rate of 2 °C min^{-1} and cooled to room temperature naturally to obtain the bioceramic scaffolds.

2.3 Material characterization

The 3D images of sintered bioceramic succulent plant-like scaffolds were reconstructed by micro-CT (SKYSCAN1172, Bruker, Germany). The microstructure of the sintered scaffolds was characterized by a scanning electron microscope (S-4800, Hitachi, Japan).

2.4 Degradation and mechanical properties of the scaffolds

The scaffolds were soaked in Tris–HCl solution (pH 7.40) at 37 °C to evaluate the degradation profile. The ratio of the solution volume to the scaffold mass was 200 mL g^{-1}. At set times of 1, 3, 7, 10, 14, 21, and 28 days, the scaffolds were taken off and dried at 60 °C overnight and the residual weight was measured. Moreover, the immersion solutions were refreshed and collected at each set time point. The concentrations of Mg and Si ions were measured with an inductively coupled plasma optical emission spectrometer (ICP, Varian 715-ES). The compressive strength of the succulent plant-like scaffolds and conventional scaffolds was measured by a universal testing machine (INSTRON-1195, INSTRON, American).

2.5 Cell culture

BMSCs were isolated from the tibia and femurs of rabbits (three weeks old) and cultured in Dulbecco's Modified Eagle's Medium low-glucose (DMEM) (Thermo Fisher Scientific, Grand Island, America) containing 10% fetal calf serum (Invitrogen) and 100 U mL^{-1} penicillin–streptomycin (Thermo Fisher Scientific), at 37 °C with 5% CO_2.

2.6 Cell viability

CCK-8 assay was performed to investigate BMSCs proliferation and viability. Briefly, 600 μL of BMSCs suspension (3×10^4 cells mL^{-1}) were seeded on each scaffold in 24-well plates and cultured for 1, 4, and 7 days. The medium was refreshed every 2 days. At each set time point, each scaffold was moved to a new 24-well plate and rinsed 3 times with PBS. The culture medium was then replaced by a culture medium with CCK-8 solution (CCK-8, Dojindo, Japan). After incubation for 1 h, the absorbance of the CCK-8 medium was measured at 450 nm wavelength in a microplate reader (SpectraFluor Plus, Tecan, Crailsheim, Germany).

2.7 Cell attachment

To evaluate the cell attachment and morphology on the scaffolds, 600 μL of BMSCs suspension (1×10^5 cells mL^{-1}) were seeded on each scaffold in a 24-well culture plate and cultured for 1, 4, and 7 days. After incubation for the set time, the scaffolds were transferred into a new 24-well culture plate and rinsed 3 times with phosphate-buffered saline (PBS) to remove the residual culture medium and the nonadherent cells. The cells were then fixed with a 4% paraformaldehyde solution for 2 h and stained with 4,6-diamino-2-phenyl indole (DAPI) and rhodamine phalloidin. The cytoskeleton was stained with phalloidin (green), and the nuclei of cells were stained with DAPI (blue). The confocal images were obtained by a confocal laser scanning microscope (Leica TCS SP8, Germany).

2.8 ALP assay

To investigate the osteogenesis-related enzymatic activity, after 7 and 14 days of incubation with different scaffolds, the Alkaline Phosphatase Assay Kit (Beyotime, China) was used to investigate the activity of alkaline phosphatase of BMSCs according to the manufacturer's instructions. Moreover, BMSCs were co-cultured with different scaffolds for 7 days in an osteogenic medium. The medium was changed every other day. The ALP activity was assessed subsequently with the BCIP/NBT Alkaline Phosphatase (ALP) Color Development Kit (Beyotime, China).

2.9 Gene expression

To evaluate the expression of osteogenesis-related genes, 600 µL of BMSCs suspension (5×10^4 cells mL^{-1}) were seeded on each scaffold in a 24-well culture plate and cultured for 4, 7, and 14 days with osteogenic differentiation medium (DMEM supplemented with 10×10^{-3} M β-glycerol phosphate, 0.2×10^{-3} M ascorbic acid, and 10% fetal bovine serum). The medium was refreshed every 3 days. After incubation for 4, 7, and 14 days, the RNA was extracted using Trizol Reagent (Invitrogen, USA). Complementary DNA (cDNA) was prepared using the PrimeScript 1st Strand cDNA synthesis kit (TOYOBO, Japan). RT-PCR was performed with the SYBR Green QPCR Master Mix (TaKaRa, Japan). The gene expression in BMSCs was evaluated and the primers used in this experiment are summarized in Table 1. GAPDH was used as the housekeeping gene.

2.10 *In vivo* bioactivity of the scaffolds

All animal experiments were approved by the Nanjing Medical University Ethics Committee and implemented according to the guidelines for animal studies (Approval number DW201902). New Zealand white rabbits (2.0–2.5 kg) were chosen and classified into 4 groups (Blank, Control, Rose, and Ellipsoid). The scaffolds (diameter = 6 mm, depth = 5 mm) were implanted into the round defects (diameter = 6 mm, depth = 5 mm) and drilled into lateral femoral condyles. All rabbits were treated with antibiotics for three days after the surgery. All rabbits were sacrificed and the samples were harvested 8 weeks after the operation.

2.11 Micro-CT

CT images of all samples were acquired *via* a Micro-CT scanner (SKYSCAN1172, Bruker, Germany). The resolution was set as 9 µm. A cylindrical region of interest (ROI, diameter: 6 mm, height: 5 mm) was chosen according to the CT data.

2.12 Histological staining

The samples were dehydrated and embedded in methyl methacrylate (PMMA). The undecalcified samples were sectioned into slices of 500 µm with a microtome (Leica, Nusseloch, Germany), and then the slices were stained with Van Gieson's picrofuchsin dye to show new bone.

Table 1 Primer sequences of genes used for quantitative real-time PCR

Genes	5′–3′	Primers
GAPDH	Forward	TCACCATCTTCCAGGAGCGA
	Reverse	CACAATGCCGAAGTGGTCGT
ALP	Forward	TGTCTGGAACCGCACTGAACTC
	Reverse	CGTGGTCAATCCTGCCTCCTTC
BMP-2	Forward	CGCCTCAAATCCAGCTGTAAG
	Reverse	GGGCCACAATCCAGTCGTT
COL-1	Forward	CTTCTGGCCCTGCTGGAAAGGATG
	Reverse	CCCGGATACAGGTTTCGCCAGTAG
OCN	Forward	CGTGGTCAATCCTGCCTCCTTC
	Reverse	AGGCGGTCTTCAAGCCATACT
RUNX2	Forward	TCAGGCATGTCCCTCGGTAT
	Reverse	TGGCAGGTAGGTATGGTAGTG

2.13 Statistical analysis

All data are displayed as the mean ± standard deviation. The statistical analysis was performed using Graphpad Prism software. The data were analyzed with *t*-tests for comparison between two groups, and one-way ANOVA for more than two groups ($*P < 0.05$, $**P < 0.01$, $***P < 0.001$, $****P < 0.0001$).

3 Results

3.1 Design and fabrication of the succulent plant-like scaffolds

To imitate the structures of succulent plants for the application of bone tissue engineering, we successfully designed the biomimetic models by imitating the macro-appearance of six types of different succulent plants (spindle shape from Graptopetalum pachyphyllum, pentagon shape from Maguey chato agave, rose shape from Aeonium canariense, triangle shape from Astroloba, ellipsoid shape from Sedum burrito, and sword shape from Echeveria Jasiri) to further investigate the osteogenic potentials (Fig. 1). Conventional scaffolds with vertical interlaced columns were prepared as the control group.

These scaffolds were successfully fabricated *via* DLP 3D printing and MgSiO$_3$ bioceramic was selected as the component of the scaffolds owing to its great biocompatibility and osteoinductivity. A column on the round base was constructed as the stem of the plants to connect the peripheral leaves. Leaves in different groups were endowed with different shapes, sizes, thicknesses, leaf areas, and curvatures according to the simplified appearances of the corresponding succulent plants.

Specifically, the Graptopetalum pachyphyllum rose is a succulent, branched at the base, with sprawling leaves like spindles; 3 layers of spindle-shaped leaves attached to the stem were stacked and rotated at 30 degrees between each layer to form the scaffold (Fig. 1A). The Maguey chato agave is a tightly formed agave with slender tepals and longer leaves than the stem. The pentagon scaffold consists of pentagon-shaped leaves like the tepals of the Maguey chato agave (Fig. 1B). The Aeonium canariense is a succulent plant with spoon-shaped leaves and smooth margins. In extreme heat, their leaves can curl to prevent excessive water loss. The rose scaffold consists of smooth spoon-shaped leaves and the interlacement space of leaves can improve nutrition storage (Fig. 1C). Astroloba has regular, sharp, triangular leaves along the symmetrical columnar stems. The triangle scaffold is composed of triangular leaves with a little stamen on the columnar stem (Fig. 1D). Sedum burrito is a succulent plant with a short stem packed with rounded leaves and this characteristic endows the plant with a small specific surface area to reduce water evaporation. Imitating the succulent, the ellipsoid scaffold consists of spherical leaves with high curvature (Fig. 1E). Echeveria jasiri grows in the shape of a solitary rosette with elongated and flat leaves. The sword-shaped scaffold consists of elongated, flat, and narrow leaves like swords (Fig. 1F). The lateral leaves are in a relatively higher position than the medial part, which could improve cell recruitment and nutrition storage.

5526 | *J. Mater. Chem. B*, 2023, **11**, 5523–5536

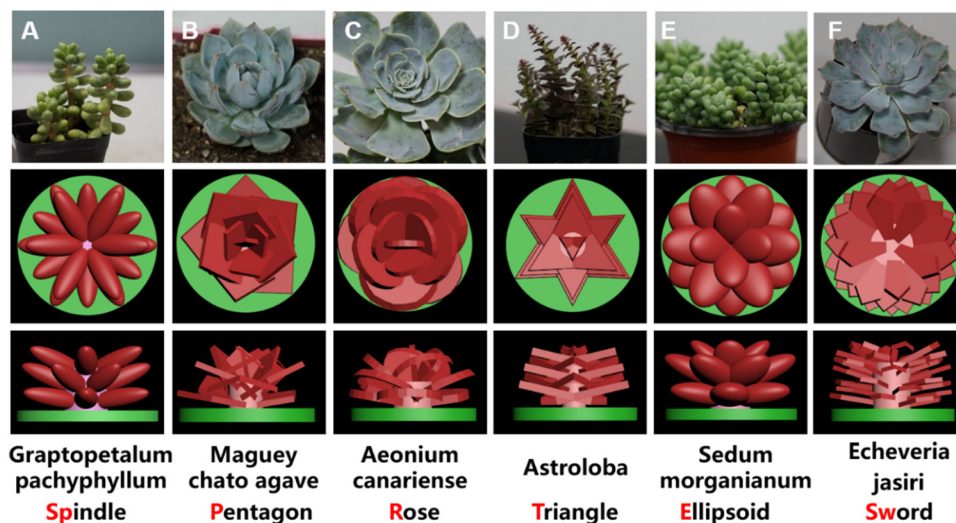This journal is © The Royal Society of Chemistry 2023

Fig. 1 Model design of biomimetic scaffolds inspired by the corresponding succulent plants. (A) The vertical and front view of spindle-shaped scaffolds designed according to the Graptopetalum pachyphyllum rose. (B) The pentagon-shaped scaffolds according to the Maguey chato agave. (C) The rose-shaped scaffolds according to the Aeonium canariense. (D) The triangle-shaped scaffolds according to the Astroloba. (E) The ellipsoid-shaped scaffolds according to the Sedum burrito. (F) The sword-shaped scaffolds according to the Echeveria Jasiri.

3.2 Characterization of the succulent plant-like scaffolds

Macroscopic images (Fig. 2B) and micro-CT images (Fig. 2C and D) show that the sintered structure was consistent with the designed model (Fig. 2A). The leaf shapes, sizes, and densities were preserved as designed. Moreover, there were no extra resin or ceramic powders left on the scaffolds. After the sintering process, the bottoms of the scaffolds were shrunken and bent but the stem and leaves of the succulent plant-like scaffolds maintained the designed structures. In addition, considerable space remained between different layers, which could be used for nutrition diffusion and cell distribution.

SEM images showed that the microstructures of the scaffolds were also consistent with the designed structure. In the central part, leaves intersected at the stem. Compared to the conventional scaffold, succulent plant-like scaffolds possessed declivate leaves with a higher outer margin than the inner part (Fig. 3A–G). However, some little cracks occurred at the intersection of leaves in the spindle group (Fig. 3B), which might be due to the sintering shrinkage caused by high temperature. Moreover, in the ellipsoid group, cracks could be observed both at the intersection and on the surface of the leaves (Fig. 3F and M). The ellipsoid leaves possessed large curvatures,
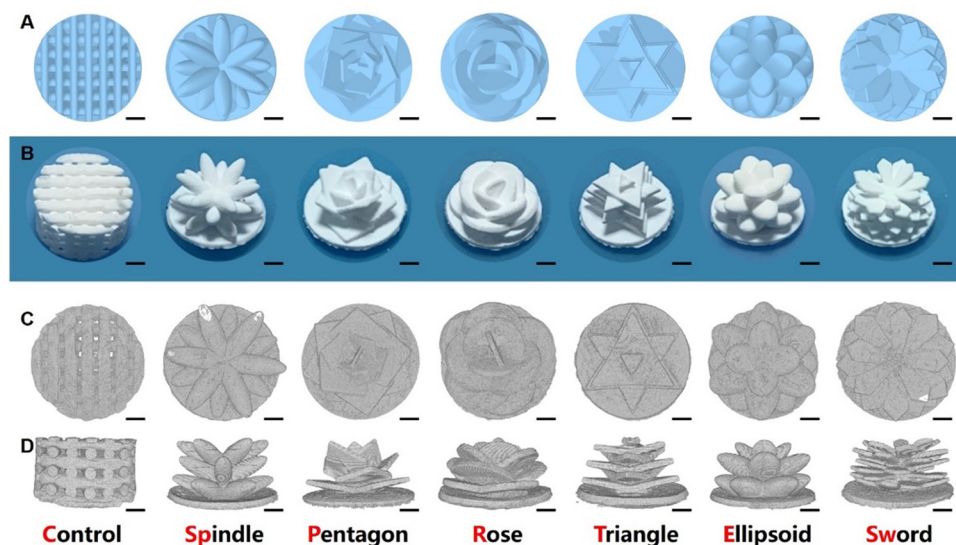

Fig. 2 Designed models and sintered succulent plant-like scaffolds. (A) Digital models applied in the 3D printing process. (B) Optical microscope images of sintered succulent plant-like scaffolds. (C) The vertical views of the CT image reconstruction show that the structures of succulent plant-like scaffolds are consistent with the designed models. Scale bar, 1 mm. (D) The side views of the CT image reconstruction present the peripheral structures of scaffolds. Scale bar, 1 mm.
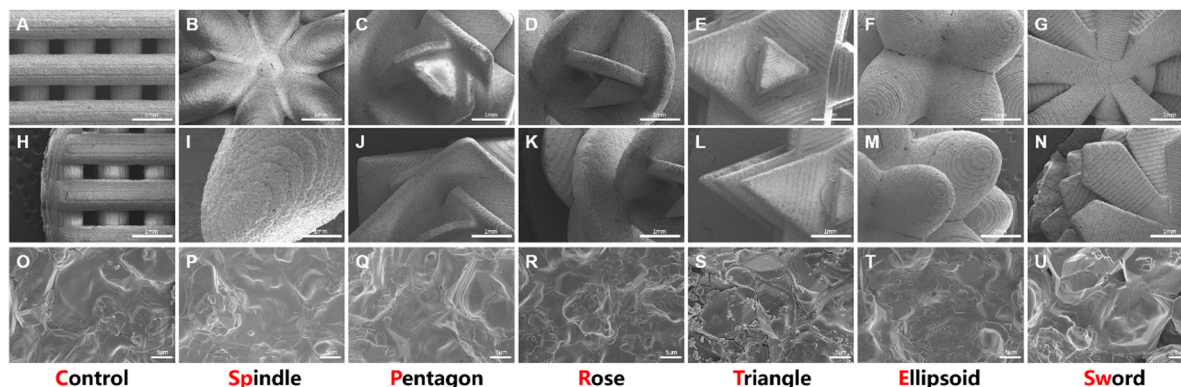
This journal is © The Royal Society of Chemistry 2023

J. Mater. Chem. B, 2023, 11, 5523–5536 | 5527

Fig. 3 SEM images of succulent plant-like biomimetic scaffolds. (A–G) The interlaced or central part of the scaffolds. Scale bar, 1 mm. (H–N) The marginal structures or leaves of the scaffolds. Scale bar, 1 mm. (O–U) The microstructure of the sintered scaffolds. Scale bar, 5 μm.

leading to more shrinkage during the sintering process than other scaffolds.

The images also show the characteristic step stripes of DLP printing (Fig. 3H–N). The dense microstructure showed well-distributed micropores and tight crystalline grain connections, which could provide stable mechanical support to load cells (Fig. 3O–U).

3.3 Degradation and mechanical profile of the scaffolds

To investigate the stability and release of ions from the scaffolds, the degradation profile was tested. All scaffolds presented a sustained release of Mg ions and Si ions (Fig. 4A and B). As compared to the experimental groups, the control group showed a faster release of Si and a faster degradation performance (Fig. 4B and C). All groups showed sustained weight loss during the Tris–HCl soaking process. After 28 days, most succulent plant-like scaffolds showed a low degradation rate (less than 5%) while the control group and spindle group showed more than 5% degradation. Fig. S1 (ESI†) shows the compressive strength of scaffolds with different macroscopic structures. The results show that the coverage compressive strength of the control group (3.56 ± 0.58 MPa) was higher than that of succulent plant-like bioceramic scaffolds (spindle 0.84 ± 0.11 MPa, pentagon 0.59 ± 0.07 MPa, rose 0.60 ± 0.09 MPa, triangle 0.60 ± 0.04 MPa, ellipsoid 1.08 ± 0.25 MPa,

and sword 0.68 ± 0.04 MPa). There was no significant difference among succulent plant-like biomimetic scaffolds with different structures.

The spindle-like scaffolds broke into pieces on day 14, illustrating that the spindle-like structure exhibited insufficient stability. The sword-shaped scaffold, with a complicated and thin leaf structure, showed weak mechanical strength due to its brittleness after sintering and broke into pieces at an early stage when soaked in Tris–HCl, so this group was ruled out from the degradation profile test.

The spindle-like scaffolds broke into pieces on day 14, illustrating that the spindle-like structure exhibited insufficient stability. The sword-shaped scaffold, with a complicated and thin leaf structure, showed weak mechanical strength due to its brittleness after sintering and broke into pieces at an early stage when soaked in Tris–HCl, so this group was ruled out from the degradation profile test.

3.4 Cell adhesion and proliferation of BMSCs in the succulent plant-like scaffolds

The attachment ability and the morphology of BMSCs on scaffolds were investigated via confocal laser scanning microscopy after 1, 4, and 7 days of incubation. As shown in Fig. 5, all groups could well support cell adhesion. On day 1, the density of cells on the scaffold was moderate and the pseudopodia
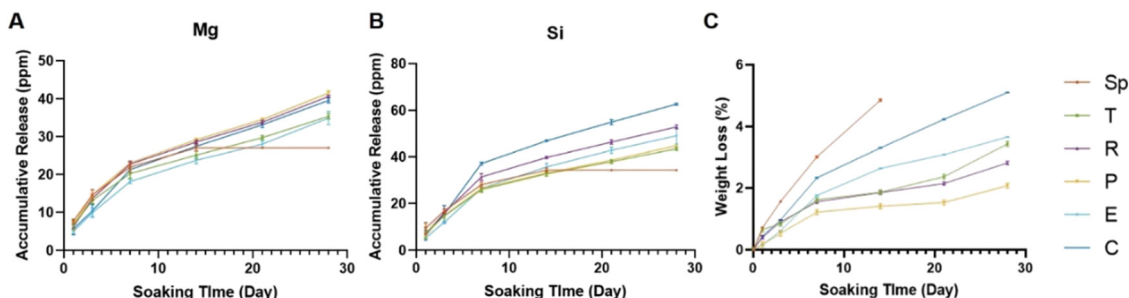

Fig. 4 Degradation profile and the weight loss of the succulent plant-like biomimetic scaffolds. (A) The accumulative release amount of Mg ions from the scaffolds in Tris–HCl solution at different time points. (B) The accumulative release amount of Si ions from the scaffolds in Tris–HCl solution at different time points. (C) The weight loss of the succulent plant-like biomimetic scaffolds and control scaffolds after soaking in Tris–HCl solution for different periods ($n = 3$).
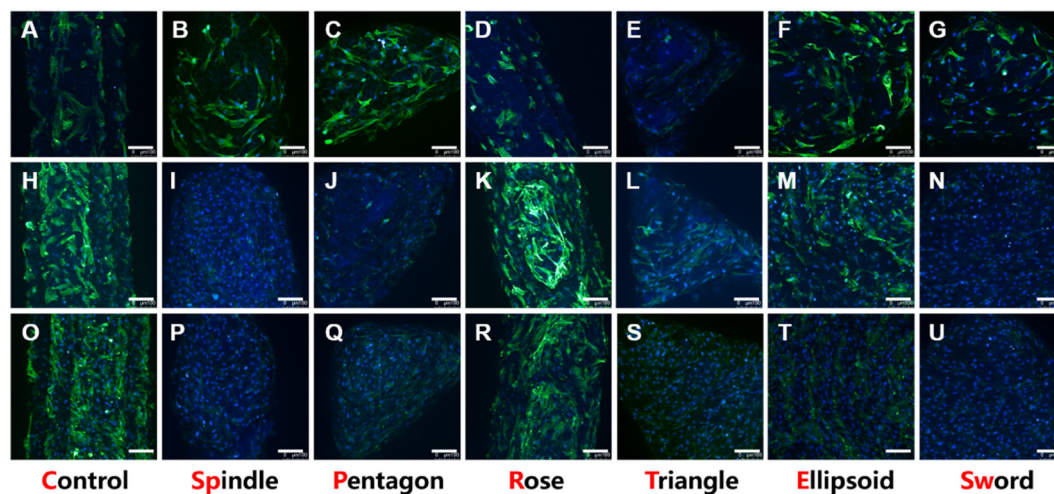
5528 | *J. Mater. Chem. B*, 2023, **11**, 5523–5536

This journal is © The Royal Society of Chemistry 2023

Fig. 5 Morphology and proliferation of BMSCs cultured in the scaffolds. (A–G) CLSM images of BMSCs adhered to the leaves of different scaffolds after 1 day of incubation. (H–N) after 4 days of incubation. (O–U) after 7 days of incubation. Scale bar, 100 μm.

adhering to the surface could be observed (Fig. 5A–G). Moreover, in the early stages of cell adhesion, the morphologies of cells in each group were different. For example, the pseudopodia of BMSCs in the spindle (Fig. 5B) and ellipsoid groups (Fig. 5F) were more elongated longer than in other groups, especially the rose group where the cells showed short and contracted pseudopodia (Fig. 5D). On day 4 (Fig. 5H–N) and day 7 (Fig. 5O–U), the cells showed a great proliferation profile, and the scaffolds were almost covered with BMSCs.

To explore the effects of $MgSiO_3$ and different structures on cell viability, BMSCs were seeded on different scaffolds and the CCK8 test was performed after 1, 4, and 7 days of incubation. The OD value at different time points showed an increase but there were no significant differences in all groups (Fig. 6A), indicating that $MgSiO_3$ had no cell toxicity and cells could proliferate well on the succulent plant-like scaffolds. Furthermore, the rate of cell adhesion was investigated to compare the cell loading efficiency on different scaffolds. Compared to the control group, the spindle, ellipsoid, and sword groups showed significantly enhanced BMSCs adhesion rates, while there was no obvious difference among the experimental groups (Fig. 6B).

3.5 *In vitro* osteogenic bioactivity of the succulent plant-like scaffolds

To investigate osteogenic differentiation, we tested the alkaline phosphatase (ALP) activity of BMSCs incubated with the scaffolds for 7 and 14 days. As shown in Fig. 6C and D, the rose-like scaffold and the ellipsoid scaffold showed significantly elevated ALP levels as compared to that in the control group after 7 and 14 days, while no significant differences were observed among other groups. According to ALP staining results, the rose-like scaffold and the ellipsoid scaffold showed relatively elevated ALP levels as compared to the control group (Fig. 6E).

Osteogenesis-related gene expression levels (*ALP*, *BMP-2*, *COL-1*, *OCN*, and *RUNX2*) were measured to evaluate the osteogenic properties of different scaffolds. For a dynamic

investigation of osteogenic properties, the gene expressions after 4, 7, and 14 days of incubation were chosen as different stages of bone formation. After 4 days of incubation, compared with the control group, succulent plant-like scaffolds, especially the rose, triangle, and ellipsoid groups, exhibited more osteogenic gene expressions such as *ALP*, *BMP-2*, *COL-1*, and *RUNX2*. Regarding the gene expression after 7 and 14 days of incubation, the general trend was that the succulent plant-like scaffolds showed more osteogenic gene expression than the control group, while on days 7 and 14, the pentagon and triangle groups showed less gene expression on *BMP-2* and *RUNX2* (Fig. 7). In particular, the rose and ellipsoid groups showed relatively higher osteogenic gene expressions than other groups. Therefore, the succulent plant-like scaffolds could improve the osteogenic differentiation of BMSCs and enhance the osteogenic gene expression as compared with the control group. Moreover, the rose and ellipsoid groups showed better osteogenic effects than all the other groups. Based on the *in vitro* osteogenic effects of the succulent plant-like scaffolds, we chose the rose and ellipsoid groups for further *in vivo* bioactivity testing.

3.6 *In Vivo* bioactivity of the succulent plant-like scaffolds

To investigate the effect of succulent plant-like scaffolds on bone repair and regeneration, rabbit femoral defect models were applied to assess *in vivo* osteogenesis. Four groups of scaffolds with different macroscopic structures were explored: Blank, Control, Rose, and Ellipsoid. Eight weeks after implantation, the samples were harvested. The 2D micro-CT images showed that the scaffolds were well placed in the defect region and could maintain the structure for eight weeks (Fig. 8A–H).

Histological analysis of Van Gieson's staining displayed the transverse slices (Fig. 8I–L) and longitudinal slices (Fig. 8M–P) of the samples. Little newly formed bone could be detected in the blank group (Fig. 8I and M). In the control group, some new bone formed around the scaffold, while little bone grew into

This journal is © The Royal Society of Chemistry 2023

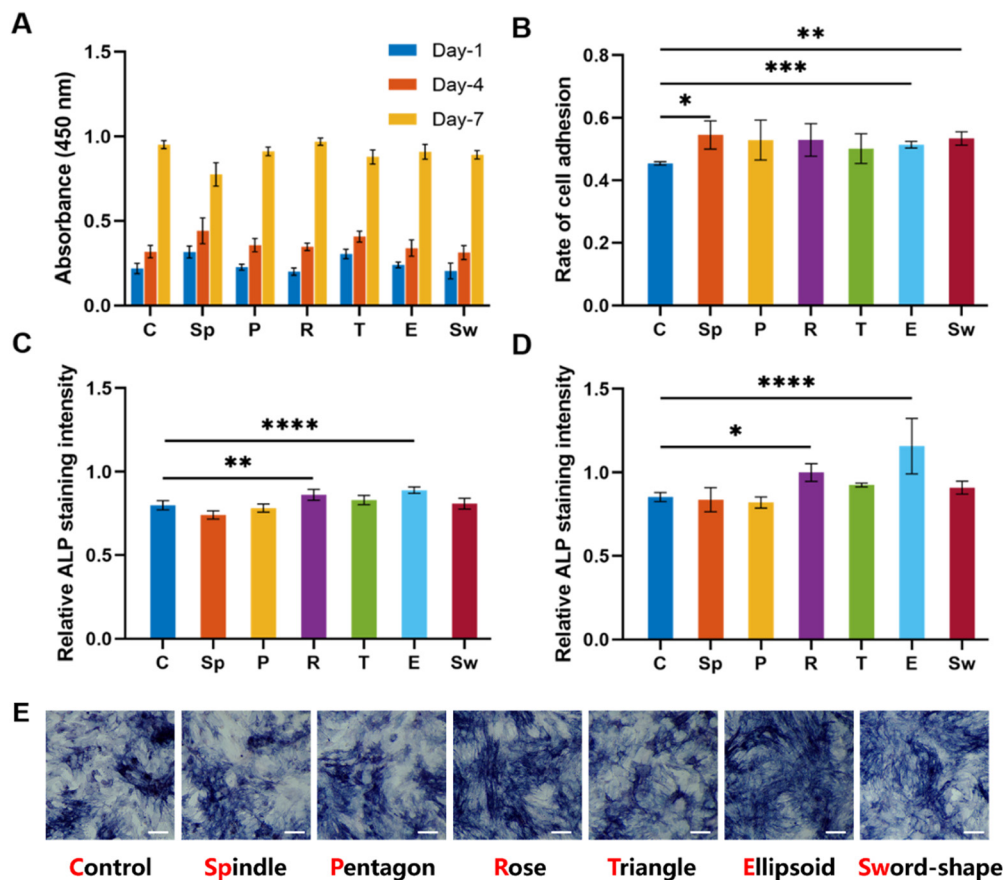*J. Mater. Chem. B*, 2023, **11**, 5523–5536 | **5529**

Fig. 6 The cell viability and ALP bioactivity of BMSCs in the succulent plant-like biomimetic scaffolds. (A) The proliferation activity of BMSCs cultured in scaffolds with different structures after culturing for 1, 4, and 7 days was detected by the CCK-8 assay. n = 5 replicates. (B) The rate of BMSCs adhesion in the different scaffolds. (C) The relative ALP activity of BMSCs cultured in different scaffolds and incubated for 7 days showed better osteogenic properties for the rose and ellipsoid groups. (D) The relative ALP activity of BMSCs cultured in different scaffolds incubated for 14 days showed better osteogenic properties for rose and ellipsoid groups. (E) The ALP staining of BMSCs co-cultured with different scaffolds for 7 days (scale bar = 20 μm) (*$P < 0.05$, **$P < 0.01$, ***$P < 0.001$, ****$P < 0.0001$).

the inner space (Fig. 8J and N). In contrast, more newly formed bone could be observed around both the rose-like and ellipsoid scaffolds, and much newly formed bone grew into the inner space of the scaffold. The gaps and cracks inside the scaffold were also filled with new bone (Fig. 8K and O). The image also suggests that parts of the scaffold degraded into some little fragments, around which a large amount of new bone had formed. Regarding the ellipsoid scaffold, more bone formed around the leaves and the ellipsoid leaves provided more contact area with peripheral tissues than the control group, making more newly formed bone attach to the surface of scaffolds (Fig. 8L). Additionally, some bone could grow into the interspace between the plant stem, leaves, and bottom (Fig. 8P). However, no bone could grow into the inner part of the scaffold due to the porous structure. The area ratio of new bone to the defect area was investigated. The quantitative analysis of the horizontal plane and vertical plane suggested that the rose-like scaffold showed significantly enhanced bone formation as compared to the control group (Fig. 8P and R).

4 Discussion

Inspired by the structures and functions of succulent plants, we designed a series of succulent plant-like scaffolds with the structures of six different plants including Graptopetalum pachyphyllum rose, Maguey Chato Agave, Aeonium canariense, Astroloba, Sedum burrito and Echeveria jasiri. The biological functions of these structures were investigated and compared to the conventional scaffolds with interlaced vertical columns. The succulent plant-like scaffolds with sophisticated structures of stems and leaves were successfully fabricated by 3D DLP printing and the morphological parameters were precisely consistent with the designed 3D models.

Many studies have focused on fabricating biomimetic scaffolds by tuning the microstructure.[29,30] The design of succulent plant-like scaffolds in this study was intended to investigate the effects of macroscopic structures on cell behavior and bone repair efficiency. Despite the brittleness of the bioceramic materials, DLP printing could offer an easy and convenient method of constructing succulent plant-like bioceramic scaffolds.
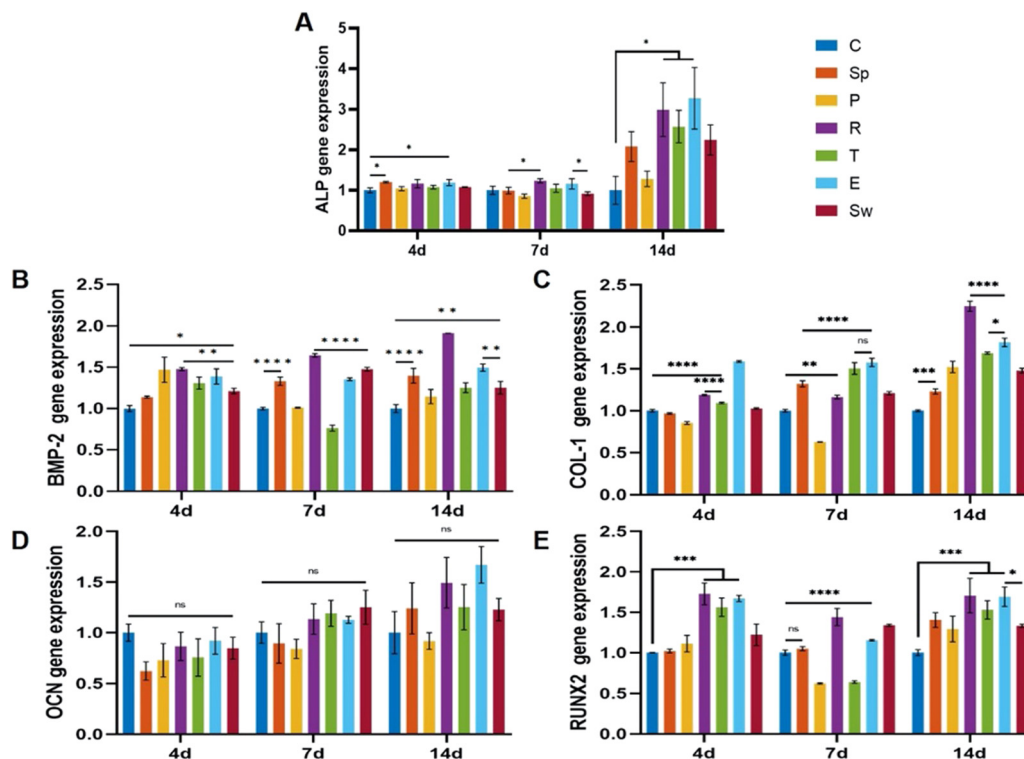
5530 | J. Mater. Chem. B, 2023, 11, 5523–5536

This journal is © The Royal Society of Chemistry 2023

Fig. 7 The succulent plant–like scaffolds showed improved osteogenic properties according to the osteogenic gene expressions after incubation for 4, 7, and 14 days. (A) The osteogenic gene expression of ALP. (B) The osteogenic gene expression of BMP-2. (C) The osteogenic gene expression of COL-1. (D) The osteogenic gene expression of OCN. (E) The osteogenic gene expression of RUNX2 (*$P < 0.05$, **$P < 0.01$, ***$P < 0.001$, ****$P < 0.0001$).

Succulent plants can be classified into the all-cell type and the storage type. The survivability of succulent plants depends on their special morphologies including stem shape, leaf shape, size, density, and specific surface area.[31–34] Naturally, the morphological transitions endow succulent plants with different water absorption and nutrition utilization capacities.[8]

Previous studies have shown that hierarchical structures of scaffolds such as multi-level pores and micro/nano-structures could play an important role in the process of tissue reconstruction and regeneration.[35,36] Physical cues including morphology, stiffness, and geometry could also regulate cell behavior *via* modulating cellular density, distribution, and interactions.[37] As such, we classified the succulent plant-like scaffolds into two types according to their different appearances. The all-cell succulent plants shared large non-spheroid leaves with oblong cross-sections and relatively high specific surface area. In contrast, the storage succulent plants had spheroid leaves with nearly round cross-sections and low specific surface areas. The former type includes pentagon, rose, triangle, and sword groups. The latter includes spindle and ellipsoid groups.

To further explore the effects of structures on cell behavior and bone repair efficiency, we customized the scaffolds by altering the leaf shape, size, and density along with the distribution of leaves according to the corresponding succulent plants. We fabricated two main types of succulent plant-like scaffolds to investigate whether different appearances would

affect cell behavior and bone regeneration. Each type also included more sub-types for further analysis. In our design, the all-cell succulents included pentagon, rose, triangle, and sword groups, which shared the same appearance with large non-spheroid leaves to increase the area for nutrition intake. The specific surface areas of the four groups were 1.56, 1.26, 1.29, and 1.53, respectively. In contrast, the storage succulents showed nearly spheroid leaves with high curvature and include spindle and ellipsoid groups. The specific surface areas of the two groups are 1.35 and 1.13.

The morphological traits endow succulent plants with different water absorption and nutrition utilization capacities by varying the leaf shape, density, and axial direction. The overlapping structure of leaves could improve fluid flow, nutrition exchanges, and contact between cells and the microenvironment.[8] The adduction structure of leaves can cause cells to aggregate on the stem and thus enhance intercellular crosstalk.[38] The leaf structure could enhance the surface area for cell adhesion and improve the distribution of cells on the leaf.[39] The short leaves with a low thickness could be formed under wet conditions, while under conditions of drought, some leaves are replaced by thorny bracts with small surface areas to reduce water evaporation.[34] Moreover, broader leaves are associated with low photosynthetic rates.[40] The increased volume of leaves may negatively impact photosynthesis due to the longer nutrition transportation distance between leaves and the stem.[33,40–42] The upregulated leaf density could decrease the water transportation efficiency due to

This journal is © The Royal Society of Chemistry 2023
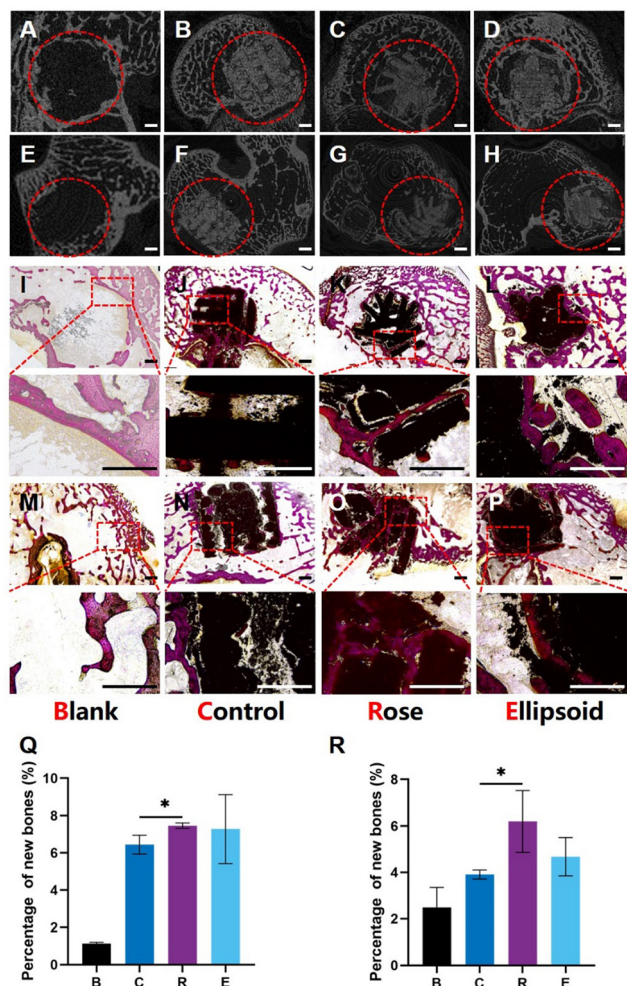
J. Mater. Chem. B, 2023, **11**, 5523–5536 | 5531

Fig. 8 The succulent plant-like biomimetic scaffolds enhanced bone regeneration in rabbit femoral defects after 8 weeks of implantation. (A–D) The 2D vertical view of the scaffolds implanted into the femoral defects. (E–H) The 2D side view of the scaffolds implanted into the femoral defects. (I–L) Transverse sections of bone defects with different scaffolds and the magnified images of the marked area. (M–P) Longitudinal sections of bone defects with different scaffolds and the magnified images of the marked area. Scale bar, 1 mm. (Q) The area ratio of the newly formed bone to defects of transverse histological slices in different groups (R) The area ratio of the newly formed bone to defects of longitudinal histological slices in different groups. (*$P < 0.05$).

the elongated path length from the veins of leaves to evaporative surfaces.[39] Moreover, studies have shown that the SA : V is the key factor that affects the living capacity in extreme environments. A low SA : V could provide the maximal volume for water storage and minimal area for transpiration water loss, so leaves with the strongest water storage capacity tend to have round cross-sections rather than planate.[4,8] Therefore, we speculated that the SA : V, leaf shapes, size, and leaf-combining methods would cooperate to affect the capacity for the absorption of nutrition and transportation in succulent plants, further modifying the viability in extreme conditions. By imitating the structures of succulent plants, the succulent plant-like scaffolds could potentially possess different capacities

for of regulating cell distribution and thus affect cell behaviors like proliferation, adhesion, and differentiation.

Here, six scaffolds with different appearances were obtained by regulating the morphology of stems and leaves *via* 3D DLP printing. The leaf shape, size, and density were preserved as designed after the sintering process, suggesting a stable method for fabricating bioceramic scaffolds with succulent plant-like structures.

Conventional porous ceramic scaffolds might face the difficulty of insufficient space for cell adhesion.[43,44] The succulent plant-like scaffolds, with a relatively smooth surface and tight crystalline grain connection, could provide a stable platform for cell adhesion and proliferation. Conventional scaffolds are composed of vertical interlaced columns, leaving a host of pores in the inner space. The pore size suitable for bone ingrowth is 300–600 μm,[45,46] which is far larger than the size of BMSCs, osteoblasts, and osteocytes. As a result, cells tend to leak from the pores, leading to a low adhesion efficiency, which might slow the speed of bone regeneration. In addition, the ECM and bioactive molecules are susceptible to being washed out from the scaffold. In contrast, the succulent plant-like scaffolds, imitating the macroscopic appearance of succulent plants, could provide more suitable cell adhesion sites and a stable microenvironment. Hopefully, our scaffolds can overcome the disadvantages of conventional scaffolds, and improve cell collection and adhesion. In addition, the intersected leaves could potentially guide cell migration for more cellular interaction and thus improve cell differentiation for osteogenesis.

$MgSiO_3$ has been verified to have the effects of enhancing cell proliferation and improving osteogenesis.[47–49] Mg ions and Si ions play important roles in the process. To explore whether the shapes affect the release profile and degradation property of scaffolds, the weight loss, and released ions were measured. We speculated that different structures would lead to different degradation properties. In succulent plants, the SA : V is the key factor that affects the capacity of water storage and evaporation. A low SA : V could help plants retain more water for survival.[4,8] Firstly, the conventional scaffolds, with the conventional porous structure, had a multitude of contact areas with the Tris–HCl solution, which might lead to fast degradation, while succulent plant-like scaffolds possessed great stability and sustained ion release. This release profile was conducive to the persistent and long-term effects on bone regeneration. The weight loss of experimental groups was in the range of 2% to 4%. The ellipsoid group, with the smallest SA : V (1.13 m^2 m^{-3}) among the succulent plant-like scaffolds, exhibited the most degradation. For plants, to retain moisture for survival, they should be in contact with more water. The ellipsoid scaffolds, imitating the structure of plants with a low SA : V, were exposed to more water than other groups, which could accelerate the degradation of the scaffolds. After 30 days of degradation testing, only 3.7% of weight loss was measured, which was enough for the bone regeneration process. Moreover, all scaffolds in our research presented the sustained and stable release of Mg and Si (30–40 ppm of Mg and 40–60 ppm of Si), which is conducive to cell adhesion, cell growth, cell differentiation,

5532 | *J. Mater. Chem. B*, 2023, **11**, 5523–5536

This journal is © The Royal Society of Chemistry 2023

activating the osteogenic signaling pathway and enhancing matrix mineralization.[27,50,51] The immune response is usually caused by free particles. In detail, broken or degraded products of scaffolds, such as nanoparticles or ceramic particles, could be recognized by macrophages, contributing to chronic inflammation and progressive tissue injury.[52] In addition, the too-fast degradation of scaffolds could lead to the burst release of scaffold components such as Mg^{2+} or other particles. The sudden increase in bioactive components in local environments might produce cell toxicity and lead to cell apoptosis and cell death, which may cause a further immune response and inflammatory response.[53,54] Thus, a stable succulent plant-like scaffold was successfully fabricated for cell growth and osteogenesis, and the stable release of bioactive components could hardly lead to an excessive immune response.

Next, the *in vitro* bioactivity was tested. The CLSM images indicated that the BMSCs could spread well on $MgSiO_3$ bioceramic scaffolds. With the increase in incubation days, the number of cells adhered to the scaffolds increased, indicating that the scaffolds could provide a suitable environment for cell adhesion and proliferation. The number of cells was less in the control group than in the experimental scaffolds, while there was no significant difference in different succulent plant-like scaffolds, which may be because cells in the control group could leak from the pores between interlaced columns.

In nature, the shapes of leaves can regulate the flow direction or aggregation of water for nutrition storage. We speculated that succulent plant-like structures could regulate cell distribution. Compared to the control group and the all-cell group, cells in the spindle and ellipsoid groups exhibited some morphology changes. Pseudopodia of BMSCs in the two groups showed greater elongation than in other groups. Previous reports have shown that substrate curvature could impose mechanical stimulation on BMSCs and induce osteogenic differentiation.[55] Thus, we speculated that the morphology of succulent plant-like scaffolds could potentially improve the BMSCs differentiation and enhance bone regeneration efficiency.

The CCK8 assays on days 1, 4, and 7 suggested that succulent plant-like scaffolds could well support cell proliferation and there was no significant difference compared with the control group, which indicated that the change in the scaffold macroscopic morphology might be a feasible method for scaffold design. Moreover, the special appearance could restrict the cells on the leaves or at the intersection places, which might enhance cell density and prevent the crowded cells from leaking from the pores of conventional scaffolds. In these conditions, the enhanced cell density could also potentially improve cellular interactions and BMSC differentiation.[56,57]

Traditionally, cells might leak from the pores of scaffolds. To investigate the capacity for cell recruitment, the cell adhesion rate was measured. The spindle, ellipsoid, and sword groups showed an enhanced cell adhesion rate compared to the control group. The three groups have structures with interlaced layers. Without many pores for cell leakage, a more effective area could be retained for cell adhesion. In other groups, cells tended to leak from the space or pores of the scaffolds, leading to a low cell loading efficiency. According to the results, the succulent plant-like scaffolds with optimal leaf structures could potentially regulate the cell adhesion efficiency and load more cells for the next repair process.

The osteogenic properties of BMSCs on different scaffolds *in vitro* and *in vivo* were investigated. Alkaline phosphate activity (ALP) is an early phenotypic marker for osteogenic differentiation.[58] The enhanced activity of ALP indicated more bone ECM (extracellular matrix) synthesis and the stimulative osteogenic differentiation effect. On days 7 and 14, the conventional scaffold showed significantly lower ALP activity than the rose-like scaffold and the ellipsoid scaffold. Moreover, osteogenesis-related gene expression levels were investigated. A significant difference was shown in different groups, suggesting that the macroscopic morphology of scaffolds might have the potential to modulate the expression of osteogenic genes. The enhanced activity and gene expression levels of ALP showed that the rose and ellipsoid groups had relatively higher osteogenic properties. In general, the expression levels of *BMP-2*, *COL-1*, and *RUNX2* indicated that the osteogenic differentiation of BMSCs in succulent plant-like scaffolds was more remarkable as compared to the control group. Previous studies reported that cellular contact could promote MSCs osteogenesis. We speculated that the succulent plant-like structure would enhance cell density and intercellular interaction by improving cell aggregation and adding the intercellular contact area. With the enhanced cell contact, the gap junction and signaling molecules between BMSCs could be activated and thus improve the osteogenic property.[59–61] Cells planted on conventional scaffolds tend to leak from the pores, leading to less cellular crosstalk and less osteogenesis. However, in succulent plant-like groups, more cells were gathered at the intersection of leaves, which could enhance the intercellular crosstalk. In addition, leaves of experimental scaffolds could provide more physical cues (large area for cell adhesion; curvature for physical cues) for cell proliferation and differentiation, which could further elevate ALP activity and osteogenesis.

The rose-like scaffold, with the adductive leaves, could gather cells into the gaps between the leaves and stems. In detail, the overlapping part of different leaves could form some deep pits and provide more space for cells to grow, which could enhance the cellular density and contact area. As reported, elevated cellular interaction could help to improve the osteogenic properties of BMSCs.[62] Moreover, the intersected and curving leaves were also conducive to cell collection and nutrition storage. The ellipsoid-like scaffold had leaves with a convex surface, providing mechanical cues like stretching strength on BMSCs. In the early stage, cells on ellipsoid scaffolds were stretched and previous reports showed that this kind of mechanical stimulation could enhance osteogenic properties.[63] In other groups, the lower layer of leaves was covered by the upper layer, which would sacrifice the contact surface between cells and scaffolds. In contrast, 3 layers of intersected leaves with different sizes in the ellipsoid group could maintain enough contact surface to load more cells.

This journal is © The Royal Society of Chemistry 2023

J. Mater. Chem. B, 2023, **11**, 5523–5536 | **5533**

The *in vivo* rabbit femoral defects models illustrated that more new bone was formed and grew in the experimental groups as compared to the control group and blank group. The micro-CT images showed that the scaffolds could still be observed with an intact appearance after two months of implantation, demonstrating that the scaffolds, having enough stability, consistent with the degradation profile, could offer long-lasting effects on osteogenesis and the period was enough for bone regeneration.[64] Furthermore, the histological analysis suggested that the succulent plant-like structure could induce bone ingrowth and bone deposition with the intersected leaves and sufficient inner space. According to *in vivo* bioactivity analysis, the experimental groups exhibited better properties on bone regeneration than the control group. It was likely that the leaf structure could provide more space for cell adhesion and prevent cells from leaking from the pores of scaffolds, which could cause more BMSCs aggregation to enhance the collagen and bone matrix deposition inside the succulent plant-like scaffolds.

Considering the further applications of succulent plant-like scaffolds, there are still some issues to be investigated. Our study only compared the effects of different shapes on BMSC osteogenic properties. More detailed parameters such as rotation angle, thickness, and inclination degree of leaves should be further investigated in the study. The mechanism of scaffold shape influence on osteogenic ability is not yet fully understood.

5 Conclusions

Inspired by the sophisticated structures of succulent plants, we have successfully fabricated biomimetic succulent plant-like scaffolds with $MgSiO_3$ bioceramic using the DLP 3D printing technology. The structures could be customized into spindle-like, pentagon-like, rose-like, triangle-like, ellipsoid-like, and sword-like appearances by changing the shape, size, and combination methods of the stems and leaves. Compared to the conventional scaffolds, the succulent plant-like scaffolds exhibited higher cell loading efficiency and more space for cellular crosstalk by gathering cells and adding a cellular contact surface. Compared to conventional 3D-printed scaffolds with vertical interlaced columns, the rose-like and ellipsoid scaffolds significantly promoted osteogenesis by elevating ALP activity after 7 days of incubation (increased by 26.5% and 30.9%, respectively, as compared to the control group) and osteogenesis-related gene expression. Furthermore, the percentage of new bone growth of rose-like scaffolds was also promoted as compared to the control group, indicating that the succulent plant-like structure had the potential to promote BMSCs differentiation for bone generation. This work provides a new biomimetic method for designing scaffolds with plant-like structures and beneficial cell microenvironments for bone regeneration.

Conflicts of interest

The authors declare no competing financial interest.

Acknowledgements

References

1 C. Feng, W. Zhang and C. Deng, *et al.*, 3D Printing of Lotus Root-Like Biomimetic Materials for Cell Delivery and Tissue Regeneration, *Adv. Sci.*, 2017, **4**, 1700401.

2 C. H. Lu, S. J. Hou and Z. Y. Zhang, *et al.*, The mystery of coconut overturns the crashworthiness design of composite materials, *Int. J. Mech. Sci.*, 2020, **168**, 105244.

3 H. W. Chen, P. F. Zhang and L. W. Zhang, *et al.*, Continuous directional water transport on the peristome surface of Nepenthes alata, *Nature*, 2016, **532**, 85–89.

4 J. Males, Secrets of succulence, *J. Exp. Bot.*, 2017, **68**, 2121–2134.

5 C. L. Ho, J. M. Chiang and T. C. Lin, *et al.*, First report of C-4/CAM-cycling photosynthetic pathway in a succulent grass, Spinifex littoreus (Brum. f.) Merr., in coastal regions of Taiwan, *Flora*, 2019, **254**, 194–202.

6 M. N. T. Le, M. Takahi and K. Ohnuma, Auto/paracrine factors and early Wnt inhibition promote cardiomyocyte differentiation from human induced pluripotent stem cells at initial low cell density, *Sci. Rep.*, 2021, **11**, 21426.

7 H. Zhang, H. Zhang and Y. Z. Xiong, *et al.*, Development of hierarchical porous bioceramic scaffolds with controlled micro/nano surface topography for accelerating bone regeneration, *Mater. Sci. Eng., C*, 2021, **130**, 112437.

8 R. M. Ogburn and E. J. Edwards, Repeated Origin of Three-Dimensional Leaf Venation Releases Constraints on the Evolution of Succulence in Plants, *Curr. Biol.*, 2013, **23**, 722–726.

9 M. Santos-Díaz, E. Balch, R. Ramírez-Malagón, *et al.*, Mexican threatened cacti: Current status and strategies for their conservation, *Species Diversity and Extinction*, 2011, pp. 1–59.

10 W. Yang, I. H. Chen and B. Gludovatz, *et al.*, Natural flexible dermal armor, *Adv. Mater.*, 2013, **25**, 31–48.

11 S. Rudykh, C. Ortiz and M. C. Boyce, Flexibility and protection by design: imbricated hybrid microstructures of bio-inspired armor, *Soft Matter*, 2015, **11**, 2547–2554.

12 D. Correa, A. Papadopoulou and C. Guberan, *et al.*, 3D-Printed Wood: Programming Hygroscopic Material Transformations, *3D Print. Addit. Manuf.*, 2015, **2**, 106–116.

13 S. Armon, E. Efrati and R. Kupferman, *et al.*, Geometry and mechanics in the opening of chiral seed pods, *Science*, 2011, **333**, 1726–1730.

14 B. Feng, M. Zhang and C. Qin, *et al.*, 3D printing of conch-like scaffolds for guiding cell migration and directional bone growth, *Bioact. Mater.*, 2023, **22**, 127–140.

5534 | *J. Mater. Chem. B*, 2023, **11**, 5523–5536

This journal is © The Royal Society of Chemistry 2023

15 J. Koffler, W. Zhu and X. Qu, *et al.*, Biomimetic 3D-printed scaffolds for spinal cord injury repair, *Nat. Med.*, 2019, **25**, 263–269.

16 P. Vashisth and J. R. Bellare, Development of hybrid scaffold with biomimetic 3D architecture for bone regeneration, *Nanomedicine*, 2018, **14**, 1325–1336.

17 M. G. Valverde, L. S. Mille and K. P. Figler, *et al.*, Biomimetic models of the glomerulus, *Nat. Rev. Nephrol.*, 2022, **18**, 241–257.

18 A. M. Al Alawi, S. W. Majoni and H. Falhammar, Magnesium and Human Health: Perspectives and Research Directions, *Int. J. Endocrinol.*, 2018, **2018**, 9041694.

19 S. Ben Zaken, Z. Radomysky and G. Koren, Association Between Serum Magnesium Levels and Alzheimer's Disease or Mixed Dementia Patients: A Population-Based Retrospective Controlled Study, *J. Alzheimer's Dis. Rep.*, 2020, **4**, 399–404.

20 J. Garg, R. Chaudhary and P. Krishnamoorthy, *et al.*, Role of Prophylactic Magnesium Supplementation in Prevention of Postoperative Atrial Fibrillation in Patients Undergoing Coronary Artery Bypass Grafting: A Meta-Analysis of 23 Randomized Controlled Trials, *J. Am. Coll. Cardiol.*, 2016, **67**, 689.

21 X. Zhou, N. Zhang and S. Mankoci, *et al.*, Silicates in orthopedics and bone tissue engineering materials, *J. Biomed. Mater. Res., Part A*, 2017, **105**, 2090–2102.

22 A. Bojovschi, M. S. Liu and R. J. Sadus, Mg2+ coordinating dynamics in Mg:ATP fueled motor proteins, *J. Chem. Phys.*, 2014, **140**, 115102.

23 H. Rubin, Central role for magnesium in coordinate control of metabolism and growth in animal cells, *Proc. Natl. Acad. Sci. U. S. A.*, 1975, **72**, 3551–3555.

24 S. Castiglioni, A. Cazzaniga and W. Albisetti, *et al.*, Magnesium and Osteoporosis: Current State of Knowledge and Future Research Directions, *Nutrients*, 2013, **5**, 3022–3033.

25 S. Ferre, E. Baldoli and M. Leidi, *et al.*, Magnesium deficiency promotes a pro-atherogenic phenotype in cultured human endothelial cells via activation of NFkB, *Biochim. Biophys. Acta*, 2010, **1802**, 952–958.

26 N. Golafshan, E. Vorndran and S. Zaharievski, *et al.*, Tough magnesium phosphate-based 3D-printed implants induce bone regeneration in an equine defect model, *Biomaterials*, 2020, **261**, 120302.

27 M. Nabiyouni, T. Bruckner and H. Zhou, *et al.*, Magnesium-based bioceramics in orthopedic applications, *Acta Biomater.*, 2018, **66**, 23–43.

28 H. Mohammadi, M. Hafezi and N. Nezafati, *et al.*, Bio-inorganics in Bioactive Calcium Silicate Ceramics for Bone Tissue Repair: Bioactivity and Biological Properties, *J. Ceram. Sci. Technol.*, 2014, **5**, 1–12.

29 J. M. Xue, C. Feng and L. G. Xia, *et al.*, Assembly Preparation of Multilayered Biomaterials with High Mechanical Strength and Bone-Forming Bioactivity, *Chem. Mater.*, 2018, **30**, 4646–4657.

30 B. Yeom, T. Sain and N. Lacevic, *et al.*, Abiotic tooth enamel, *Nature*, 2017, **543**, 95–98.

31 D. Cicuzza, D. S. Staheli and R. Nyffeler, *et al.*, Morphology and Anatomy Support a Reclassification of the African Succulent Taxa of Senecio Sl (Asteraceae: Senecioneae), *Haseltonia*, 2017, 11–26.

32 H. Griffiths and J. Males, Succulent plants, *Curr. Biol.*, 2017, **27**, R890–R896.

33 X. Noblin, L. Mahadevan and I. A. Coomaraswamy, *et al.*, Optimal vein density in artificial and real leaves, *Proc. Natl. Acad. Sci. U. S. A.*, 2008, **105**, 9140–9144.

34 H. Akhani, M. Ghasemkhani and S. D. Chuong, *et al.*, Occurrence and forms of Kranz anatomy in photosynthetic organs and characterization of NAD-ME subtype C4 photosynthesis in Blepharis ciliaris (L.) B. L. Burtt (Acanthaceae), *J. Exp. Bot.*, 2008, **59**, 1755–1765.

35 Y. Liu, S. Yang and L. Cao, *et al.*, Facilitated vascularization and enhanced bone regeneration by manipulation hierarchical pore structure of scaffolds, *Mater. Sci. Eng., C*, 2020, **110**, 110622.

36 M. Xu, D. Zhai and L. Xia, *et al.*, Hierarchical bioceramic scaffolds with 3D-plotted macropores and mussel-inspired surface nanolayers for stimulating osteogenesis, *Nanoscale*, 2016, **8**, 13790–13803.

37 K. Metavarayuth, P. Sitasuwan and X. Zhao, *et al.*, Influence of Surface Topographical Cues on the Differentiation of Mesenchymal Stem Cells in Vitro, *ACS Biomater. Sci. Eng.*, 2016, **2**, 142–151.

38 H. Griffiths, Plant venation: from succulence to succulents, *Curr. Biol.*, 2013, **23**, R340–R341.

39 R. M. Ogburn and E. J. Edwards, Quantifying succulence: a rapid, physiologically meaningful metric of plant water storage, *Plant, Cell Environ.*, 2012, **35**, 1533–1542.

40 T. J. Brodribb, T. S. Feild and G. J. Jordan, Leaf maximum photosynthetic rate and venation are linked by hydraulics, *Plant Physiol.*, 2007, **144**, 1890–1898.

41 L. Sack and K. Frole, Leaf structural diversity is related to hydraulic capacity in tropical rain forest trees, *Ecology*, 2006, **87**, 483–491.

42 C. K. Boyce, T. J. Brodribb and T. S. Feild, *et al.*, Angiosperm leaf vein evolution was physiologically and environmentally transformative, *Proc. R. Soc. B*, 2009, **276**, 1771–1776.

43 H. Y. Chang, W. H. Tuan and P. L. Lai, Biphasic ceramic bone graft with biphasic degradation rates, *Mater. Sci. Eng., C*, 2021, **118**, 111421.

44 M. A. Kafi, K. Aktar and Y. Phanny, *et al.*, Adhesion, proliferation and differentiation of human mesenchymal stem cell on chitosan/collagen composite scaffold, *J. Mater. Sci.: Mater. Med.*, 2019, **30**, 131.

45 N. Taniguchi, S. Fujibayashi and M. Takemoto, *et al.*, Effect of pore size on bone ingrowth into porous titanium implants fabricated by additive manufacturing: An in vivo experiment, *Mater. Sci. Eng., C*, 2016, **59**, 690–701.

46 Q. Ran, W. Yang and Y. Hu, *et al.*, Osteogenesis of 3D printed porous Ti6Al4V implants with different pore sizes, *J. Mech. Behav. Biomed. Mater.*, 2018, **84**, 1–11.

47 S. H. Lin, G. Z. Yang and F. Jiang, *et al.*, A Magnesium-Enriched 3D Culture System that Mimics the Bone

This journal is © The Royal Society of Chemistry 2023

J. Mater. Chem. B, 2023, **11**, 5523–5536 | 5535

Development Microenvironment for Vascularized Bone Regeneration, *Adv. Sci.*, 2019, **6**, 1900209.

48 S. Shi, W. T. Fan and R. Tao, *et al.*, Natural Bio-mineralization-Inspired Magnesium Silicate Composite Coating Upregulates Osteogenesis, Enabling Strong Anterior Cruciate Ligament Graft-Bone Healing In Vivo, *ACS Biomater. Sci. Eng.*, 2021, **7**, 133–143.

49 S. Vahabzadeh, M. Roy and S. Bose, Effects of silicon on osteoclast cell mediated degradation, in vivo osteogenesis and vasculogenesis of brushite cement, *J. Mater. Chem. B*, 2015, **3**, 8973–8982.

50 G. Turnbull, J. Clarke and F. Picard, *et al.*, 3D bioactive composite scaffolds for bone tissue engineering, *Bioact. Mater.*, 2018, **3**, 278–314.

51 J. R. Henstock, L. T. Canham and S. I. Anderson, Silicon: the evolution of its use in biomaterials, *Acta Biomater.*, 2015, **11**, 17–26.

52 S. Gordon, Phagocytosis: An Immunobiologic Process, *Immunity*, 2016, **44**, 463–475.

53 K. J. Rambhia and P. X. Ma, Controlled drug release for tissue engineering, *J. Controlled Release*, 2015, **219**, 119–128.

54 X. Huang and C. S. Brazel, On the importance and mechanisms of burst release in matrix-controlled drug delivery systems, *J. Controlled Release*, 2001, **73**, 121–136.

55 S. J. Lee and S. Yang, Substrate Curvature Restricts Spreading and Induces Differentiation of Human Mesenchymal Stem Cells, *Biotechnol. J.*, 2017, **12**, 1700360.

56 J. Zhang, E. Wehrle and P. Adamek, *et al.*, Optimization of mechanical stiffness and cell density of 3D bioprinted cell-laden scaffolds improves extracellular matrix mineralization and cellular organization for bone tissue engineering, *Acta Biomater.*, 2020, **114**, 307–322.

57 R. Peng, X. Yao and B. Cao, et al., The effect of culture conditions on the adipogenic and osteogenic inductions of mesenchymal stem cells on micropatterned surfaces, *Biomaterials*, 2012, **33**, 6008–6019.

58 M. J. Li, X. L. Fu and H. C. Gao, *et al.*, Regulation of an osteon-like concentric microgrooved surface on osteogenesis and osteoclastogenesis, *Biomaterials*, 2019, **216**, 119269.

59 A. S. Mao, J. W. Shin and D. J. Mooney, Effects of substrate stiffness and cell-cell contact on mesenchymal stem cell differentiation, *Biomaterials*, 2016, **98**, 184–191.

60 M. Nouri-Goushki, L. Angeloni and K. Modaresifar, *et al.*, 3D-Printed Submicron Patterns Reveal the Interrelation between Cell Adhesion, Cell Mechanics, and Osteogenesis, *ACS Appl. Mater. Interfaces*, 2021, **13**, 33767–33781.

61 J. Tang, R. Peng and J. Ding, The regulation of stem cell differentiation by cell-cell contact on micropatterned material surfaces, *Biomaterials*, 2010, **31**, 2470–2476.

62 L. Zhang, G. J. Jiao and S. W. Ren, *et al.*, Exosomes from bone marrow mesenchymal stem cells enhance fracture healing through the promotion of osteogenesis and angiogenesis in a rat model of nonunion, *Stem Cell Res. Ther.*, 2020, **11**, 38.

63 L. L. Yang, Q. Gao and L. Ge, *et al.*, Topography induced stiffness alteration of stem cells influences osteogenic differentiation, *Biomater. Sci.*, 2020, **8**, 2638–2652.

64 E. F. Morgan, A. Giacomo and L. C. Gerstenfeld, Overview of Skeletal Repair (Fracture Healing and Its Assessment), *Methods Mol. Biol.*, 2021, **2230**, 17–37.

5536 | *J. Mater. Chem. B*, 2023, **11**, 5523–5536

This journal is © The Royal Society of Chemistry 2023